LARGE EDDY SIMULATION OF NATURALLY INDUCED FIRE WHIRLS IN A VERTICAL SQUARE CHANNEL WITH CORNER GAPS

by

B. Farouk
Department of Mechanical Engineering and Mechanics
Drexel University
Philadelphia, PA 19104, USQ
and
K.B. McGrattan and R.G. Rehm
Building and Fire Research Laboratory
National Institute of Standards and Technology
Gaithersburg, MD 20899, USA

Reprinted from the **International Mechanical Engineering Congress and Exposition (IMECE) Proceedings. Modeling and Numerical Simulation of Combustion Processes Session. November 5-10,2000, Orlando, FL, 2001.**

NIST
National Institute of Standards and Technology
Technology Administration, US. Department of Commerce

To be presented at the IMECE, Orlando, Florida, November 6 – 10,2000
(Session on Modeling and Numerical Simulation of Combustion Processes)

LARGE EDDY SIMULATION OF NATURALLY INDUCED FIRE WHIRLS IN A VERTICAL SQUARE CHANNEL WITH CORNER *GAPS*

B. Farouk, K. B. McGrattan* and R G. Rehm*
Department of Mechanical Engineering and Mechanics
Drexel University
Philadelphia, PA 19104

'Building and Fire Research Laboratory
National Institute of Standards and Technology
Gaithersburg, MD 20899

ABSTRACT

Naturally occurring fire whirls are rare but highly destructive phenomena. These are mostly generated by the interaction between a buoyant fire plume and its surroundings. The whirling motion generated can enhance the plume length and sustain burning. In this paper, we report the results of a numerical investigation of whirling fires generated in vertical square channels with symmetric comer gaps. The numerical investigations of swirling fire plumes are used to analyze how the comer gaps alters the plume dynamics and combustion. An approximate (low Mach number) form of the Navier-Stokes equations is solved to calculate the mixing and transport of combustion products. Large scale eddies are directly simulated and sub-grid scale motion is represented with a Smagorinsky model. The current approach is based on a fixed heat release rate, regardless of the strength of the whirl generated by the corner slots. The effect of corner slot widths and their configuration on the swirling motion are studied systematically for a given channel geometry and fixed fuel-loss rate.

Key words: Fire whirls, large eddy simulations

NOMENCLATURE

c_p	constant pressure specific heat
d	channel length and width
d_c	lateral gap between channel walls
h	enthalpy
g	gravitational acceleration
k	thermal conductivity
L	channel height
P	pressure
$\dot{q}$	heat release rate
t	time
T	temperature
u	velocity vector
u,v	velocity components along x, y directions
w	velocity component in the z direction
x,y	coordinates along the horizontal plane
r	radial coordinate
z	coordinate in the vertical direction
Z_c	vertical clearance between the floor and the channels

Greek symbols

ΔH_c	heat of combustion of fuel
ρ	density
τ'	stress tensor
θ	azimuthal coordinate
ν	kinematic viscosity
γ	ratio of specific heats

INTRODUCTION

Naturally occurring fire whirls are rare but highly destructive phenomena. These are mostly generated by the interaction between the buoyant fire plume and its surroundings, The whirling motion generated can enhance the plume length and sustain burning. In large-scale urban fires, the presence of neighboring structures can cause fire whirls – which in turn can cause extensive damage.

Emmons and Ying (1967) conducted one of the earliest studies to investigate the fire whirl phenomena. A fire whirl from a liquid-fuel pool (acetone) was formed at the center of a rotating screen which imparted a controlled angular momentum to the ambient air. Measurements showed that the fire whirl consists of a rotating cylinder, fuel rich inside, and lean outside. The flame was observed to lengthen vertically and tighten radially with increasing screen rotation. Recently Battaglia et al. (1999) investigated the same problem numerically to further understand how swirl alters the plume dynamics and combustion. A review by Morton (1970) describes the underlying mechanisms which produce and sustain a fire whirl.

Satoh and Yang (1996) conducted experimental observations of fires based on self-generated swirling flows to study some aspects of the whirling fires found in large urban and forest fires. In their study, swirl was caused by channeling the entrainment flows caused by the fire itself located in a square enclosure with symmetric corner gaps. The qualitative effects of different fuels, sizes of the fuel pan relative to that of the enclosure, and the wall gap sizes were

also studied. The elongated flame height of the whirling fires is a strong function of the heat release rate, which depends on the volatility of the
fuel. The flame height was found to vary directly with the fuel-loss rate. They observed that for fuels of decreasing volatility, the whirling flame height decreased accordingly. Satoh and Yang (1997) also attempted to simulate the self-generated whirling fires by an approximate fire field model. A k-e turbulence model was used. In addition volumetric heat release was confined within a vertical column to mimic the combustion in a plume. In another recent study, Satoh and Yang (1999) provide quantitative observations using both a high-speed motion camera and a thermographic infrared camera for self-generated whirling fires from a single flame in a vertical enclosure with comer gaps.

There have only been a few studies to theoretically model fire whirls – self generated or mechanically induced. Due to the complex interaction of the fire whirl with the fuel source and fuel consumption, most of these studies have not been able to adequately reproduce experimental observations.

A numerical investigation of self-generated swirling frre plumes (in a vertical square enclosure with symmetric comer gaps) is reported in this paper. A methodology has been developed to model fires with the use of efficient flow solving techniques and high spatial and temporal resolution (McGrattan et al., 1998). An approximate form of the Navier-Stokes equations is solved to calculate the mixing and transport of combustion products. Large scale eddies are directly simulated and sub-grid scale motion is represented with a Smagorinsky (1963) model. The fire is prescribed in a manner consistent with a mixture-fraction based approach to combustion. The present model and computational methodology have reproduced mean temperature and buoyant velocity correlations for large fire plumes in the absence of swirling (McCaffrey, 1979; Baum and McCaffrey, 1989).

PROBLEM DESCRIPTION

A fire source is centrally located at the base of a square channel with dimensions of 0.64 m x 0.64 m in the horizontal plane, as shown in Figure 1. The channel is open at the top. Each channel wall (0.05 m thick) has a uniform lateral gap at its comers so that entrained air (due to the buoyancy of the burning flame) can enter into the channel through the four corner gaps. The entrained air (in the form of wall jets) thus can impart a rotational flow to interact with the rising buoyant flame. The height of the channel walls extended up to 1.8 m, however, finite vertical gaps between the floor and the walls were also considered (as seen in Figure 1). The computational domain (1.0 m x 1.0 m x 1.9 m) extended beyond the channel dimensions to realistically simulate the fire plume within a square enclosure with corner and bottom gaps.

MODEL DESCRIPTION

The simulations of the fire plume are based on the schematic shown in Figure 1. The fire plume is a three-dimensional transient buoyant flow that can be modeled by the motion of a thermally expandable ideal gas (Rehm and Baum, 1978). The Navier-Stokes equations are solved for such a fluid driven by a prescribed heat source, where

$$\frac{\partial \rho}{at} + \nabla \cdot \rho \mathbf{u} = 0 \qquad (1)$$

$$\rho\left(\frac{\partial \mathbf{u}}{\partial t} + \mathbf{u} \cdot \nabla \mathbf{u}\right) + \nabla p - \rho \mathbf{g} = \nabla \cdot \tau \qquad (2)$$

$$\frac{\partial \rho h}{\partial t} + \nabla \cdot \rho h \mathbf{u} - \frac{dp_0}{dt} = \dot{q}''' + \nabla \cdot (k \nabla T + \dot{q}^R) \qquad (3)$$

$$p_0(t) = \rho T R \qquad (4)$$

The fluid variables are density p, velocity u, pressure p, gravity g, viscous stress tensor τ, enthalpy h, volumetric heat release rate $\dot{q}'''$, thermal conductivity k, temperature T, radiant energy flux q^R, and universal gas constant R .

Following Rehm and Baum (1978) the pressure is decomposed into three components, a background (average) pressure $p_0(t)$, a hydrostatic contribution $-\rho_0 gz$, and a perturbation to the hydrostatic pressure $\tilde{p}(x,t)$. The subscript 0 is a reference value of density, and z is the vertical coordinate. Equations (3) and (4) are modified using the background pressure p_0 which depends on time only. In this manner, high-frequency acoustic oscillations are eliminated while large temperature and density variations typically found in fues are retained. The resulting equations are thus referred to as weakly compressible and are valid for low Mach number flows.

Constant pressure specific heat of the gas is considered to be independent of temperature, giving

$$h = c_p T$$

Combining the conservation equations for mass (1), energy (3) and state (4) results in an expression for the divergence of the flow $\nabla \cdot \mathbf{u}$

$$p_0(t) \nabla \cdot \mathbf{u} + \frac{1}{\gamma} \frac{dp_0}{dt} = \frac{\gamma - 1}{\gamma} [\dot{q}''' + \nabla \cdot (k \nabla T + \dot{q}^R)] \qquad (5)$$

Equation (5) is integrated over the entire domain for pressure p_0 and is used as a consistency condition.

The momentum equation (2) is simplified by subtracting off the hydrostatic pressure gradient, and then dividing by the density to obtain

$$\frac{\partial \mathbf{u}}{\partial t} + \frac{1}{2} \nabla |\mathbf{u}|^2 - \mathbf{u} \times \omega + \frac{1}{\rho_0} \nabla \tilde{p} = \frac{1}{\rho} [(\rho - \rho_0) \mathbf{g} + \nabla \cdot \tau] \qquad (6)$$

where ω is the vorticity. Introducing the head H, the final form of the momentum equation is

$$\frac{\partial \mathbf{u}}{\partial t} - \mathbf{u}\times\boldsymbol{\omega} + \nabla H = \frac{1}{\rho}[(\rho-\rho_0)\mathbf{g} + \nabla\cdot\tau] \qquad (7)$$

where

$$\nabla H = \frac{1}{2}\nabla|\mathbf{u}|^2 + \frac{1}{\rho_0}\nabla\tilde{p}$$

The quantity $1/\rho_0$ implies that the vorticity generation induced by buoyancy is much more important than that due to the baroclinic effects, i. e. the non-alignment of the pressure and density gradients. The pressure perturbation is solved by taking the divergence of the momentum equation, which results in an elliptic partial differential equation for H,

$$\nabla^2 H = -\frac{\partial(\nabla\cdot\mathbf{u})}{\partial t} - \nabla\cdot\mathbf{F} \qquad (8)$$

where the convective and diffusive terms have been incorporated in the term **F**.

a eddy t techniaue

The equations presented above can be solved directly to i a solution to the problem of a buoyant fire plume. The difficulty arises in that the length and time scales associated with the fluid dynamics and combustion y over orders of magnitude In order to t the dynamics of the problem, models for τ l q''' are necessary. h goal i t ture mixing on scales where the d l viscosity is significant – which ll requires a very grid to resolve. Alternate approaches include the use of Reynolds- ged of the governing e ti tankar, 1980) or tl use of a gi scale i (large eddy simulation). The eraged form of the s (e.g. the k-e turbulence , have a l limitation for fire p – he avera procedure at the r of the model a The k-ε was developed as a time-averaged approximation to the conservation equations of fluid dynamics. While the precise nature of the averaging time is not , it is clearly long enough to t f large eddy p coefficients describe the unresolved fluxes of mass, u and gy. This is the rir au of the smoothed appearance of t results of re the most ly h e fire ns e s e length s are determined t e product of the local and t averaging time, rather than the spatial resolution of the underlying p grid. Infortunately, the evolution of large eddy ti of most fire plumes is lost l an ap as is the l t trans events.

The t of the large eddy tion (LES) niqu to fire is aimed t g r l and t l lit from simulations of fire performed on the r finely meshed grids allowed by modem fast computers. The basic idea behind the LES i is that the eddies that account for most of the mixing are large enough to be calculated with reasonable accuracy from the equations of fluid dynamics. The small scale eddy motion is modeled via a sub-grid description. One such representation is the Smagorinsky model (1963) where the sub-grid scale Reynolds stress tensor is given by

$$\tau_{ij} = \max[\mu_{lam}, \rho(C_s\Delta)^2|S|].(\frac{\partial u_i}{\partial x_j} + \frac{\partial u_j}{\partial x_i} - \delta_{ij}\frac{2}{3}\frac{\partial u_k}{\partial x_k}) \qquad (9)$$

where μ_{lam} is the laminar viscosity and Cs is an empirical constant, A is a length on the order of the grid cell size and

$$|S| = 2(\frac{\partial u}{\partial x})^2 + 2(\frac{\partial v}{\partial y})^2 + 2(\frac{\partial w}{\partial z})^2 + (\frac{\partial u}{\partial y} + \frac{\partial v}{\partial x})^2 + (\frac{\partial u}{\partial z} + \frac{\partial w}{\partial x})^2 + (\frac{\partial v}{\partial z} + \frac{\partial w}{\partial y})^2 \qquad (10)$$

There have been numerous refinements of the original Smagorinsky model but it is difficult to assess the improvements offered by the newer schemes. There are two reasons for this. First, the structure of the fire plume is dominated by the large scale resolvable eddies, so that even a constant eddy viscosity gives results almost identical with those obtained with the Smagorinsky scheme (Baum et al., 1997). Second, the lack of precision in most large-scale fire data makes it difficult to sort out the subtleties associated with these models. In this study, we have used the Smagorinsky model with $C_s = 0.14$, which produces satisfactory results for most large-scale applications where boundary layers are not important.

Combustion model

A sub-grid thermal element model (TEM) is formulated to represent the fire. A large number of Lagrangian particles are introduced into the plume, releasing heat as they are convected by the thermally induced motion (Baum et al., 1994; McGrattan et al., 1998). The combustion and hydrodynamics are coupled here since the fluid motion determines where the heat is released, while the heat release determines the motion. The concept is based on mixture-fraction theory for the transport of a conserved scalar that describes a reacting species. The TEM requires that the burning rate be prescribed as an input into the calculation. It is intended for applications where small-scale mixing and diffusive processes that control non-premixed combustion cannot be resolved on the grid used to perform the simulations.

The overall heat release rate $\dot{q}$ from the fire is discretized as thermal elements that represent pyrolized fuel. At a specified surface, such as the fuel bed, thermal elements

are ejected at a rate of $\dot{n}''$ particles per unit time per unit area. The heat release rate of a single thermal element is given by

$$\dot{q}_{p,j} = \frac{\dot{q}''}{\dot{n}''}\frac{1}{t_b} \qquad (11)$$

where $\dot{q}''$ is the heat release rate per unit area of the fuel bed and t_b is the burnout time ($t - t_0 < t_b$) of the thermal element and t_0 is the time the element is ejected from the burning surface. The burnout time is obtained fiom the plume correlations of Baum and McCaffrey (1989). It is assumed that the thermal element burns out somewhere in the intermittent region of the plume, $1.3D^* < z' < 3.30D^*$ where z' is the height above the firebed, $D^* = [\dot{q}/(\rho_0 c_p T_0 \sqrt{g})]^{\frac{2}{5}}$ is the characteristic diameter of the fire, and $\dot{q}$ is the total heat release of the fire. The burnout time falls somewhere between $1.05\sqrt{D^*/g} < t_b < 1.86\sqrt{D^*/g}$ and is usually a few tenths of a second. The heat release term in equation (3) is the summation of convective heat release rates of the individual thermal elements in a grid cell of volume $\delta x \delta y \delta z$.

$$\dot{q}''' = \frac{\sum \dot{q}_{p,j}}{\delta x \delta y \delta z}$$

Boundary Conditions

No-slip boundary conditions are used for the floor and the vertical walls of the enclosure. The computational domain extends beyond the square channel in all three directions. All enclosure walls and floor are considered to be thermally adiabatic. Open boundary conditions are used along the top and the vertical sides of the computational domain. The fire source is located at the center of the enclosure (0.2 m x 0.2 m) on a 0.05 m pedestal. As discussed earlier, thermal elements are ejected fiom the burning surface, and burned at a prescribed rate. The thermal elements are introduced with a velocity, which is calculated from the heat release rate flux, the density of the fuel gases ρ_f, and the heat of combustion of fuel ΔHc,

$$w_n = \frac{\dot{q}_f''}{\rho_f \Delta Hc} \qquad (12)$$

At open external boundaries it is assumed that the perturbation pressure is zero.

NUMERICAL FORMULATION

The governing 'equations (1 – 3) and the Poisson equation for the total pressure (8) are numerically solved. The combustion is simulated via the thermal element model as described in the previous section. The spatial derivatives are discretized with second-order central differencing and a second-order Runge-Kutta scheme is used to advance the velocity and temperature fields. The linear algebraic system arising fiom the discretization of the Poisson equation has constant coefficients and can be solved to machine accuracy by direct (non-iterative) methods that utilize the fast Fourier transform and block tri-diagonal solvers. The grid is rectangular with uniform spacing in the vertical direction and slight stretching in the horizontal directions. The discretization for a computational cell is based on staggered-gridding techniques.

RESULTS AND DISCUSSION

The simulations of the whirling fires are based on the schematic shown in Figure 1. The computational domain is a rectangular region with square base (1.0 m x 1.0 m) and a height of 1.9 m. The origin of the Cartesian coordinate system is at the front left comer. Thus the center of the base is at x = 0.5 m, y = 0.5 m. The burner specifications represent a fuel source yielding 20.0 kW fire. The fire strength was ramped to its full strength within an interval of 1 s and held at 20.0 kW thereafter. For the present calculations, only 65% of the energy fiom combustion is considered to be the convective heat release. The rest of the energy, converted to radiation, did not play any role in the simulations as none of the surfaces were specified as thermally-thick or thermally-thin. The heating value of the fuel (ΔHc) was taken as 42,000 kJ/kg.

Though past studies have indicated that whirl initiation can increase the fuel consumption rate, no attempt was made in this study to couple the two. It is also reported that fuel volatility (and the fuel gas velocity at the burning surface) has a direct effect on the flame elongation for whirling plumes. Fixed heat release was considered for all simulations, regardless of the whirl strength. It is also noted that the effect of fuel volatility is not considered in the present formulation. The fuel gas velocity at the burning surface (equation 12) does not specifically consider fuel volatility.

Analogous to experiments by Satoh and Yang (1996, 1999), whirl can be induced by simulating a fire within a square vertical enclosure with symmetric corner gaps. In addition to the lateral gaps (d_c) between the enclosure walls, we also considered vertical clearance (Z_c) between the floor and the enclosure walls. It was found that both d_c and Z_c significantly affects the predicted plume dynamics and the entrained flow field within the enclosure.

Numerical tests were performed to determine the grid size necessary to resolve the flowfield with accuracy. Simulations were carried with three grid sizes, 32 x 32 x 64, 48 x 48 x 72 and 64 x 64 x 96. Little variation of the time-averaged results were observed between the grid sizes 48 x 48 x 64 and 64 x 64 x 96. All results presented in this paper are thus for a grid size of 48 x 48 x 72. An average

simulation takes approximately 18 μs per time step per cell on an SGI Octane 195 MHz processor and requires about 12000 time steps for 20 s of simulation time. All simulations reported in this paper were carried out for 100 s. This was found to be adequate time for the flow to reach quasi-steady state.

The present model was first applied to simulate an open fire plume – without any enclosure walls. The time-dependent solutions capture the intermittency of the flame, and plume zones as discussed in Baum and McCaffrey (1989). Time-averages of the outputs of this kind of simulation produce a smoother image of the flame. The time-averaged temperature and axial (z-component) velocity variation along the centerline (x=0.5 m, y = 0.5 m) is shown in Figure 2. The time-averaged centerline temperature and axial velocity profiles have been found to compare well with McCaffrey's (1979) correlation, except near the base, where the present model over-predicts the temperature. The reason for this is that the mesh spanning the burner is relatively coarse, but fairly typical of most practical calculations where the fire plume comprises only a small fraction of the total volume of the computational domain.

The fire plume was then simulated within an enclosure with symmetric comer gaps (d_c = 0.1 m). Each wall was placed on the floor with no vertical clearance (Z_c = 0.0 m) and extended up to 1.8 m in height. Visualization of the computed time-dependent flow field revealed that very quickly the flame began to rotate about the enclosure vertical axis as the entrained air flowing through the lateral gaps reached the fire. The flame leaned towards the inside walls of the enclosure as it precessed and was unable to stand straight up. Instead of elongating, the plume became shorter along the centerline. The dynamics of the plume motion for this case is shown in Figure 3 where the time variation of the angular velocity (v_θ) and temperature at an off-axis location (x = 0.71 m, y = 0.28 m) at a height of 0.9 m are shown. As the flame rotates, leaning towards the inside walls of the enclosure, the temperature at the above location periodically increases. The angular velocity also undergoes similar fluctuations as the flame undergoes a precessional motion. The axial variation of the time-averaged (between 50 s and 100 s) entrainment flux through the lateral gap is shown in Figure 4. The entrainment flux at the base of the enclosure is rather high. The horizontal velocities of the entrained flow is found to be significantly higher than the fuel gas velocity at the burning surface, given by equation (12). The high entrainment velocities at the burner surface thus destabilize the fire plume and induce the precessional motion. The time-averaged temperature and axial (z-component) velocity variation along the centerline (x=0.5 m, y = 0.5 m) is shown in Figure 5. Due to the precessional motion, the plume shortens considerably along the centerplane. Both the temperature and the axial velocity along the centerline undergo drastic changes compared to similar results shown for the open plume.

Simulations were carried out by systematically varying the lateral gap width (from 0.05 m to 0.3 m while maintaining zero vertical clearance between the floor and the enclosure walls. For all cases, precessional motion of the flame was strong and no elongation of the plume was predicted.

Simulations were then carried out for enclosures with both corner gaps between walls and vertical gaps between the floor and the walls. A stable and elongated plume is predicted for the case where d_c = 0.1 m and Z_c = 0.5 m. The vertical gap allows the fire plume to attain a high vertical velocity before encountering the wall jets entrained by the comer gaps. The entrained flow entering the enclosure through the comer gaps induces a whirling motion to the plume along the vertical axis.

The effect of varying the vertical gap width on the fire plume was investigated next, keeping the lateral gap width d_c = 0.1 m. A stable and elongated plume was also predicted for the case where d_c = 0.1 m and Z_c = 0.25 m. The coupling of the vertical plume velocity and the horizontal entrained jets at the bottom of the enclosure walls favors the formation of an elongated plume in this case. A slightly longer plume is observed when Z_c = 0.25 m compared to the plume predicted for Z_c = 0.5 m. . The time-averaged temperature and axial (z-component) velocity variation along the centerline (x=0.5 m, y = 0.5 m) is shown in Figure 6. Very little difference is observed between the temperature profiles shown in Figure 2 (open fire plume) and in Figure 6. The axial velocity at the exit is however, much higher in the present case than that in the open plume. This is perhaps due to the fixed heat release rate calculation being carried out. It has been reported in the literature (Satoh and Yang, 1996) that an elongated and radially tightened plume increases the heat release rate.

The time averaged velocity vectors at a horizontal plane (z = 0.6 m) for the above case is shown in Figure 7. The blank regions in the figure outline the location of the enclosures. The corner jets entrained by the lateral gaps are clearly shown. As the four jets enter the enclosure, they interact with the rising column of the fire plume and form four co-rotating vortices. These vortices provide both stability and stretching of the fire plume. The central region of the fire plume, however, does not show any pronounced rotation. Due to the presence of the four co-rotating vortices at the comers, the plume remains straight and tight. Unlike the case reported in Figures 3 – 5, the plume does not precess and lean at the enclosure walls. Figure 8 shows the time variation of the angular velocity (v_θ) at an off-axis location (x = 0.71 m, y = 0.28 m) at a height of 0.9 m. The radial location of this point is 0.3 m fiom the vertical axis of the computational domain. Since the flow-structure within the enclosure is rather complex (see discussion on Figure 7 above), the angular velocities shown in Figure 7 is not the swirl velocity of the core of the fire plume itself.

Calculations were carried out by further reducing the vertical clearance, Z_c to 0.125 m while keeping the lateral gap

width d_c at 0.1 m. A stable slender plume is observed in this case also, however, the elongation is somewhat smaller than the case with Z, = 0.25. The time averaged velocity vectors at a horizontal plane (z = 0.6 m) for this case (Z_c = 0.125 m , d_c = 0.1 m) is shown in Figure 9. The comer jets entrained by the lateral gaps are again clearly seen. A strong rotating flow field is seen in the region close to the walls, however, the four co-rotating vortices are still present. Due to the smaller vertical clearance, the buoyant plume is somewhat weak when it encounters the entrained wall jets.

Finally results are presented for a case where the lateral gap width is further reduced to d_c = 0.05 m and the vertical clearance Z, = 0.25 m. The time-averaged temperature and axial velocity variation along the centerline is shown in Figure 10. The narrow lateral gap produces faster jets entering the enclosure. Also due to adequate vertical clearance, the buoyant jet attains high velocity before encountering the entrained flow. The result is a longer fire plume as seen in the above two figures.

CONCLUSIONS

Numerical simulations of fire plumes located in vertical square channels with corner and vertical gaps were conducted. The present LES methodology for simulating fires is based on direct solution of the large scales and sub-grid scale approximations for the dynamic viscosity and heat release.

The simulations were based on fixed heat release rate and fixed fuel gas inlet-velocity conditions for the burning surface. The present results provide interesting insights to the coupling mechanism of a buoyant plume with lateral entrainment jets generated by the comer gaps in the enclosure. The results also reveal possible flow structures in the enclosure that inhibit precession of the fire plume and provide stability. The effect of varying the lateral comer gap width and the vertical clearance between the floor and the enclosure walls on the plume dynamics was also explored.

Future studies are planned to address the feedback of the elongated plume on the fuel consumption rate and the fuel volatility.

ACKNOWLEDGEMENTS

One of the authors (BF) gratefully acknowledges support from the Building and Fire Research Laboratory at NIST, Gaithersburg, MD where he served as a Guest Researcher during the academic year 1999-00

REFERENCES

Baum, H. R., and McCaffrey, B. J., 1989, 'Fir Induced Flow Field – Theory and Experiment' Fire Safety Science – Proceedings of the Second International Symposium, pp. 129-148

Baum, H. R., Ezekoye, O. A., McGrattan, K. B., and Rehm, R. G., 1994, 'Mathematical Modeling and Computer Simulation of Fire Phenomena', Theoretical and Computational Fluid Dynamics, Vol. 6(2-3), pp. 125-139

Baum, H. R., McGrattan, K. B., and Rehm, R. G., 1997, 'Three Dimensional Simulations of Fire Plume Dynamics', Fire Safety Science – Proceedings of the Fifth International Symposium, pp. 511-522

Battaglia, F., McGrattan, K. B., Rehm, R. G. and Baum, H. R., 'Simulating Fire Whirls', NIST Internal Report 6341, July 1999

Emmons, H. W. and Ying, S. J., 1967, 'The Fire Whirl', Eleventh Symposium (International) on Combustion, pp. 475-488

McCaffrey, B. J., 1979, 'Purely Buoyant Diffusion Flames: Some Experimental Results' National Bureau of Standards Report

McGrattan, K.B., Baum, H. R. and Rehm, R. G., 1998, 'Large Eddy Simulation of Smoke Movement', Fire Safety Journal, Vol. 30(2), pp. 161-178

Morton, B. R., 1970, 'The Physics of Fire Whirls', Fire Research Abstracts and Reviews, Vol. 12(1), pp. 1-19

Patankar, S. V., 1980, Numerical Heat Transfer and Fluid Flow, Hemisphere Publishing, New York

Rehm, R. G. and Baum, H. R., 1978, The Equations of Motion of Thermally Driven Buoyant Flows, Journal of Research, National Bureau of Standards, Vol. 83(3), pp. 297-308

Soma, S. and Saito, K., 1991, Reconstruction of Fire Whirls using Scale Models, Combustion and Flames, Vol. 86, pp. 269-284

Satoh, K. and Yang, K. T., 1996, 'Experimental Observations of Swirling Fires ', ASME HTD-Vol. 335, pp. 393-400

Satoh, K. and Yang, K. T., 1997, 'Simulations of Swirling Fires Controlled by Channeled Self-generated Entrainment Flows', Fire Safety Science, - Proceedings of the Fifth International Symposium, pp. 201-212

Satoh, K. and Yang, K. T., 1999, 'Measurement of Fire Whirls from a Single Flame in a Vertical Square Channel with Symmetrical Corner Gaps', ASME HTD-Vol. 364-4, pp. 167-173

Smagorinsky, J., 1963, 'General Circulation Experiments with Primitive Equations, I. The Basic Experiments', Monthly Weather Review, Vol. 91, pp. 99-164

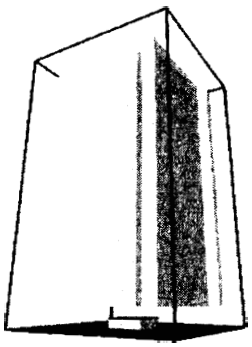

Figure 1. Schematic of the problem geometry

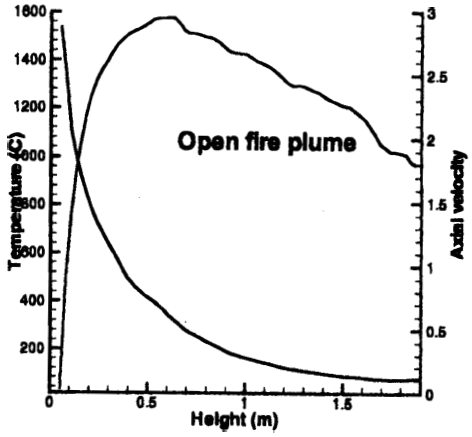

Figure 2. Time-averaged temperature and axial velocity profiles along the vertical direction (x = 0.5 m, y = 0.5 m) for the open plume

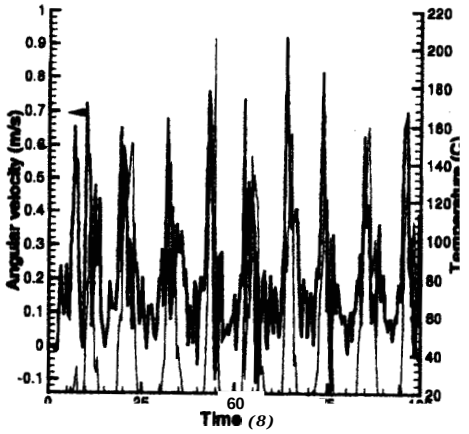

Figure 3. Temporal variation of the angular velocity and temperature at a given location within the enclosure (x = 0.71 m, y = 0.28 m, z = 0.9 m) for a partially enclosed plume (d_c = 0.1 m, Zc = 0.0)

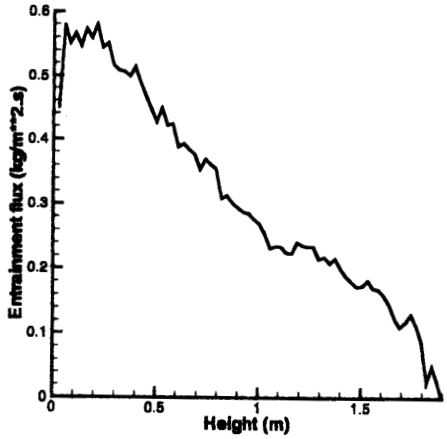

Figure 4. Time-averaged entrainment flux through the lateral gap for a partially enclosed plume (d_c = 0.1 m, Zc = 0.0)

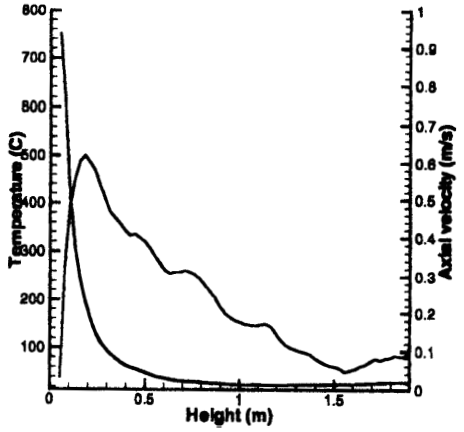

Figure 5. Time-averaged temperature and axial velocity profiles along the vertical direction (x = 0.5 m, y = 0.5 m) for a partially enclosed plume (d_c = 0.1 m, Zc = 0.0)

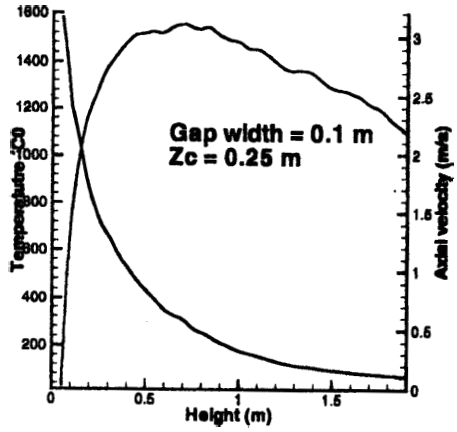

Figure 6. Time-averaged temperature and axial velocity profiles along the vertical direction (x = 0.5 m, y = 0.5 m) for a partially enclosed plume (d_c = 0.1 m, Zc = 0.25 m)

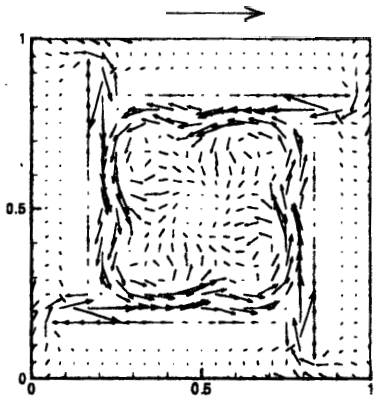

Figure 7. Time-averaged velocity field at z = 0.6 m for a partially enclosed plume (d_c = 0.1 m, Zc = 0.25 m)

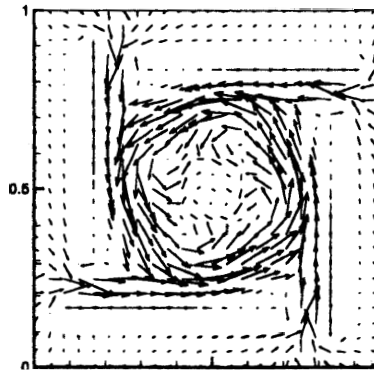

Figure 9. Time-averaged velocity field at z = 0.6 m for a partially enclosed plume (d, = 0.1 m, Zc = 0.125 m)

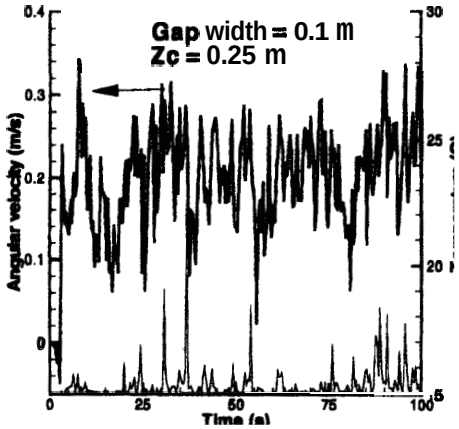

Figure 8. Temporal variation of the angular velocity and temporature at a given location within the enclosure (x = 0.7m, y = 0.28 m, z = 0.9 m) for a partially enclosed plume (d_c = 0.1 m, Zc = 0.25 m)

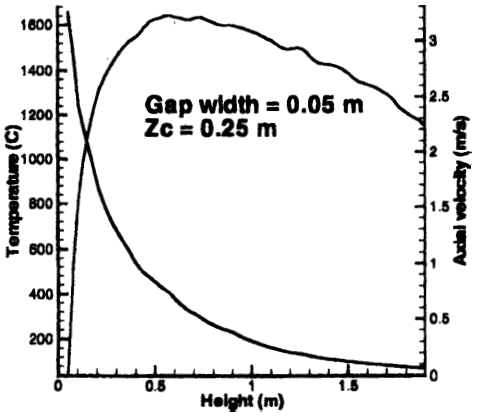

Figure 10. Time-averaged temperature and axial velocity profiles along the vertical direction (x = 0.5 m, y = 0.5 m) for a partially enclosed plume (d_c = 0.05 m, Zc = 0.25 m)